EUROPEAN ORGANIZATION FOR NUCLEAR RESEARCH

CERN-PH-EP/2004-049
September 3, 2004

Measurement of Exclusive $\rho^0\rho^0$ Production in Mid-Virtuality Two-Photon Interactions at LEP

The L3 Collaboration

Abstract

Exclusive $\rho^0\rho^0$ production in two-photon collisions between a quasi-real and a mid-virtuality photon is studied with data collected at LEP at centre-of-mass energies 183 GeV $< \sqrt{s} <$ 209 GeV with a total integrated luminosity of 684.8 pb^{-1}. The cross section of the process $\gamma\gamma^* \to \rho^0\rho^0$ is determined as a function of the photon virtuality, Q^2, and the two-photon centre-of-mass energy, $W_{\gamma\gamma}$, in the kinematic region: 0.2 GeV$^2 < Q^2 <$ 0.85 GeV^2 and 1.1 GeV $< W_{\gamma\gamma} <$ 3 GeV.

Submitted to *Phys. Lett. B*

1 Introduction

Recently, the L3 Collaboration measured the processes $\gamma\gamma^* \to \rho^0\rho^0$ and $\gamma\gamma^* \to \rho^+\rho^-$, where one of the interacting photons, γ, is quasi-real and the other, γ^*, is off-mass-shell and has a virtuality in the range $1.2\ \mathrm{GeV}^2 < Q^2 < 30\ \mathrm{GeV}^2$ [1, 2]. The cross sections of these isospin-related reactions have a similar dependence on the two-photon centre-of-mass energy, $W_{\gamma\gamma}$, and are of similar magnitude, though the $\rho^+\rho^-$ cross section is systematically higher than the $\rho^0\rho^0$ one. These features of ρ pair-production at high Q^2 are in contrast with the observed suppression, and different $W_{\gamma\gamma}$ dependence, of $\rho^+\rho^-$ production [3] with respect to $\rho^0\rho^0$ [4, 5] in the data for $Q^2 \approx 0$ and $W_{\gamma\gamma} < 2$ GeV.

The observed behaviour of ρ pair-production at large momentum transfer is well described by the QCD-based model developed in Reference 6, as shown by the analysis of the L3 data presented in Reference 7. On the other hand, ρ pair-production by quasi-real photons is still not well understood, despite a wide range of theoretical models [8, 9]. Thus, the study of the Q^2 evolution of ρ pair-production between these two Q^2 regimes is an important task in the experimental investigation of vector meson pair-production in two-photon interactions. This Letter presents results on the measurement of the process:

$$\mathrm{e^+e^-} \to \mathrm{e^+e^-}\gamma\gamma^* \to \mathrm{e^+e^-}\rho^0\rho^0 \tag{1}$$

in a kinematic region of intermediate values of the squared momentum transfer:

$$0.2\ \mathrm{GeV}^2 < Q^2 < 0.85\ \mathrm{GeV}^2 \tag{2}$$

and for an invariant mass of the hadronic system, $W_{\gamma\gamma}$, in the interval:

$$1.1\ \mathrm{GeV} < W_{\gamma\gamma} < 3\ \mathrm{GeV}. \tag{3}$$

The data sample used was collected by the L3 detector [10] at LEP at centre-of-mass energies $183\ \mathrm{GeV} < \sqrt{s} < 209\ \mathrm{GeV}$ and corresponds to an integrated luminosity of $684.8\ \mathrm{pb}^{-1}$. Scattered beam electrons[1)] which have radiated photons with virtualities in the range (2) can be detected ("tagged") by the Very Small Angle Tagger (VSAT) [11]. The VSAT is an electromagnetic calorimeter made of BGO crystals installed around the beam line on opposite sides of the L3 detector, at 8.05 m from the interaction point. Its geometrical acceptance covers the polar angle range $5\ \mathrm{mrad} < \theta < 10\ \mathrm{mrad}$, for azimuthal angles in the ranges $-1.25\ \mathrm{rad} < \phi < 1.25\ \mathrm{rad}$ and $\pi - 1.25\ \mathrm{rad} < \phi < \pi + 1.25\ \mathrm{rad}$. When the electron with the largest scattering angle is detected by the VSAT, the maximum virtuality of the two photons, Q^2, is, to good approximation, equal to the transverse momentum squared, p_t^2, of the final state hadron system:

$$Q^2 = 2E_bE_s(1 - \cos\theta_s) \approx E_bE_s\theta_s^2 \approx p_t^2\,, \tag{4}$$

where E_b is the beam energy, and E_s and θ_s are the energy and the scattering angle of the tagged electron, respectively. The VSAT provides a means to ensure selection of exclusive final states by correlating the scattered electron and the detected hadron system.

The $\rho^0\rho^0$ production cross section is determined as a function of $W_{\gamma\gamma}$ and Q^2. The results are compared to the generalised vector dominance model (GVDM) [12]. A measurement of process (1) in a similar kinematic region was performed at lower centre-of-mass energy by the PLUTO Collaboration [5]. The present measurement represents a tenfold increase of the statistics compared to that measurement.

[1)] Throughout this Letter, the term "electron" denotes both electrons and positrons.

2 Event Selection

The reaction (1), contributing to the process

$$e^+e^- \to e^+e^-_{tag}\pi^+\pi^-\pi^+\pi^- \,, \tag{5}$$

is identified by a scattered electron, e_{tag}, detected in the VSAT and four charged pions measured in the tracking chamber. These events are collected by two independent track-triggers [13]. The trigger efficiency is determined from the data itself, making use of the redundancy of the triggers, and is around 94%.

Single-tagged events are selected by requiring one electromagnetic cluster in the VSAT. This cluster must have energy greater than 50% of the beam energy in order to reduce the background and to ensure a sufficient containment of the electromagnetic shower.

The event candidates must have exactly four tracks with zero total charge. All tracks must come from the interaction vertex, have transverse momentum greater than 100 MeV and an energy loss in the tracking chamber compatible with the pion hypothesis.

Events containing muons are removed from the selected data sample. A search for secondary vertices is performed and events with reconstructed neutral kaons are also rejected. Energy depositions above 60 MeV in the electromagnetic calorimeter, not associated with a charged track, are selected as photons. An event is allowed to contain no more than one such photon with energy below 300 MeV which should not exceed 10% of the total energy of the four-pion system. Events containing higher-energy photons are discarded.

According to equation (4), the transverse momentum squared p_t^2 of the four-pion system is used to measure the Q^2 of the event. It is required to be in the range (2). For an exclusive final state, the projections of the momentum vectors of the electron tag and the four-pion system on to the plane perpendicular to the beam direction must be back-to-back. Therefore, the acoplanarity angle, ϕ_{aco}, calculated from the difference between the azimuthal angles of the tagged electron and the four-pion system, is required to be less than 0.4 rad, as shown in Figure 1a.

After all cuts, 1958 events are observed. Their four-pion mass spectrum is shown in Figure 2a. The region (3) is populated by 1836 events, which are used for the cross section determination. The mass distribution of the $\pi^+\pi^-$ combinations of the selected events, displayed in Figure 2b, shows a strong ρ^0 signal. A prominent clustering of entries is observed at the crossing of the ρ^0 mass bands in the correlation plot of the masses of the neutral $\pi^+\pi^-$ combinations, shown in Figure 2c. No such resonance structure is observed in the correlation plot of the masses of the $\pi^+\pi^+$ and $\pi^-\pi^-$ combinations, presented in Figure 2d. These features of the two-particle mass correlations give evidence for a signal from $\rho^0\rho^0$ intermediate states.

We also inspect the two- and three-pion mass distributions in the data for production of higher-mass resonances. The only statistically significant evidence is for production of the $f_2(1270)$ resonance, which appears in the two-pion mass spectra in the intervals 2.1 GeV $< W_{\gamma\gamma} <$ 2.5 GeV and 2.5 GeV $< W_{\gamma\gamma} <$ 3 GeV as illustrated in Figure 3. Measurement of $f_2(1270)$ production is beyond the scope of the present study, which is concentrated on ρ^0 pair-production.

3 Monte Carlo Modelling and Studies

To estimate the number of $\rho^0\rho^0$ events in the selected four-pion data sample, we consider non-interfering contributions from the processes:

$$\begin{aligned} &\gamma\gamma^* \to \rho^0\rho^0\,; \\ &\gamma\gamma^* \to \rho^0\pi^+\pi^-\,; \\ &\gamma\gamma^* \to \pi^+\pi^-\pi^+\pi^-\,, \text{ non}-\text{resonant}. \end{aligned} \tag{6}$$

To take into account $f_2(1270)$ production in the region $W_{\gamma\gamma} > 2.1$ GeV, we also consider contributions from the processes:

$$\begin{aligned} &\gamma\gamma^* \to f_2 f_2\,; \\ &\gamma\gamma^* \to f_2\rho^0\,; \\ &\gamma\gamma^* \to f_2\pi^+\pi^-. \end{aligned} \tag{7}$$

Monte Carlo samples of processes (6) and (7) are generated with the EGPC [14] program. About 4 million events are produced for each of the processes (6), about 3 million events for the first of the processes (7) and 1.6 million events for the two remaining processes. The $W_{\gamma\gamma}$ and Q^2 dependence are those of the $\gamma\gamma$ luminosity function [15] and only isotropic production and phase-space decays are included. The generated events are passed through the full L3 detector simulation using the GEANT [16] and GEISHA [17] programs and then processed in the same way as the data, reproducing the detector behaviour as monitored in the different data-taking periods. The scattered electrons are propagated from the interaction point to the VSAT taking into account the influence of the magnetic field of the L3 solenoid and the LEP quadrupole magnets installed between the L3 detector and the VSAT [11].

For acceptance calculations, Monte Carlo events are assigned a Q^2-dependent weight, evaluated using the GVDM form-factor [12] for both photons. The detection efficiencies of process (1), calculated taking into account the detector acceptance and the efficiency of the selection procedure, are in the range of $2\% - 4\%$ and are listed in Tables 1 and 2 in different Q^2 and $W_{\gamma\gamma}$ intervals. The efficiency is mostly limited by the kinematics of the two-photon reaction which boosts the hadronic system along the beam direction, often resulting in low-angle tracks outside the fiducial tracking volume. This geometric acceptance is then further reduced by the limited angular coverage of the VSAT. The detection efficiencies for the other subprocesses from (6) are of the same magnitude as the $\rho^0\rho^0$ one and follow a similar evolution with Q^2 and $W_{\gamma\gamma}$. Including the $f_2(1270)$ branching fraction into two charged pions, the detection efficiencies for the $\gamma\gamma^* \to f_2\rho^0$ and $\gamma\gamma^* \to f_2\pi^+\pi^-$ processes are of the order of 2% and the detection efficiency of the $\gamma\gamma^* \to f_2 f_2$ process is about 1.2%.

For Monte Carlo events passing the selection, the generated energy of the tagged electron always exceeds 90% of the beam energy, with an average $< E_s/E_b > = 0.987$. This ensures that the approximation of Q^2 by p_t^2, given by relation (4), is valid within 1% in the region (2). The Q^2 resolution is determined by the measurement of p_t^2 and varies between 8% and 10%; the resolution on $W_{\gamma\gamma}$ is better than 3%.

4 Background Estimation

The contribution to the selected sample from e^+e^- annihilation is negligible. Using 2 million Monte Carlo events of the reaction $e^+e^- \to e^+e^-\tau^+\tau^-$ generated with the program LEP4F [18],

the background contribution from this process is estimated to be 0.6 ± 0.3 events and is neglected. The background is mainly due to partially reconstructed events from two-photon interactions with higher particle multiplicities in the final state, when tracks or photons escape detection. Another background contribution arises from "fake tags", *i.e.* random coincidences with off-momentum beam electrons, which give a signal in the VSAT. These signals correspond to energy depositions comparable with the beam energy, and are thus not removed by the cut on the energy of the VSAT cluster.

To estimate the background due to feed-down from higher-multiplicity final states, we select a data sample of doubly-charged four-pion events, $\pi^+\pi^+\pi^+\pi^-$ and $\pi^+\pi^-\pi^-\pi^-$, in which at least two charged particles are undetected. In addition, we also select $\pi^+\pi^-\pi^+\pi^-\pi^0$ events which are used to account for background events with undetected neutral pions.

All these events are required to pass the event selection procedure, releasing the charge-conservation requirement for the doubly-charged events and considering only the $\pi^+\pi^-\pi^+\pi^-$ subsystem of the $\pi^+\pi^-\pi^+\pi^-\pi^0$ events. The ϕ_{aco} distributions of the accepted background-like data events are combined with the distribution of selected $\pi^+\pi^-\pi^+\pi^-$ Monte Carlo events so as to reproduce the ϕ_{aco} distribution observed in data. The result of this procedure, applied for the events in the kinematic region defined by (2) and (3), is shown in Figure 1. The resulting background levels are quoted in Tables 1 and 2.

Dedicated studies show that the off-momentum beam particles at the VSAT location are dominantly on the outer side of the LEP ring. Therefore, the related background would appear as an excess in the number of events having a tag on the outer side of the accelerator ring, N_{out}, with respect to the inner side, N_{in}. This feature is observed, for instance, in data when the cut on ϕ_{aco} is released, as shown in Figure 1b. In the selected data, displayed in Figure 1c, the ratio $N_{out}/N_{in} = 1.02 \pm 0.05$ is close to unity, indicating that the background from fake tags is small. The ratio of the number of selected events having tag in the forward versus backward directions along the beam line, 1.04 ± 0.05, is also compatible with unity. We note that since the two background-like data samples used in the background estimation originate from real physics processes, they contain a fraction of events with fake tags and take into account the effect of this background.

5 Fit Method

In order to determine the differential $\rho^0\rho^0$ production rate, a maximum likelihood fit of the data to the sum of the processes (6) and (7) is performed in intervals of Q^2 and $W_{\gamma\gamma}$.

The parameter set, Ω, comprising the six two-pion masses in an event, namely the four neutral combinations $\pi^+\pi^-$ and the two doubly-charged combinations $\pi^\pm\pi^\pm$, provides a complete kinematic description of a four-pion event in our model of isotropic production and decay. For each data event, i, with measured variables Ω_i, we calculate the probabilities, $P_j(\Omega_i)$, that the event resulted from the j-th production mechanisms of the six possible ones as listed in (6) and (7). A likelihood function is defined as:

$$\Lambda = \prod_i \sum_{j=1}^{6} \lambda_j P_j(\Omega_i)\,, \qquad \sum_{j=1}^{6} \lambda_j = 1, \tag{8}$$

where the fit parameter λ_j is the fraction of process j in the $\pi^+\pi^-\pi^+\pi^-$ sample for a given Q^2 or $W_{\gamma\gamma}$ bin and the product runs over all data events in that bin. The probabilities P_j are determined by the six-fold differential cross sections of the corresponding process, using Monte Carlo samples and a box method [19].

In the fits we assume that the processes (7) involving $f_2(1270)$ production contribute only for $W_{\gamma\gamma} > 2.1$ GeV, as suggested by the spectra in Figure 3. We find the f_2 content in the data to be well described by the $f_2\pi^+\pi^-$ and $f_2\rho^0$ contributions only. Therefore, in order to reduce the correlations between the fitted parameters and their uncertainties, we exclude the process $\gamma\gamma^* \to f_2 f_2$ from further consideration. Thus, we perform a five-parameter fit in the Q^2 bins and in the $W_{\gamma\gamma}$ bins for the region $W_{\gamma\gamma} > 2.1$ GeV, whereas the fits in the $W_{\gamma\gamma}$ bins for $W_{\gamma\gamma} < 2.1$ GeV have three parameters and take into account only contributions from the processes (6).

As a check of the fit method, we find that the maximum-likelihood fit reproduces the $\rho^0\rho^0$ content of Monte Carlo test samples within statistical uncertainties. Since the analysis procedure is optimised for deriving the $\rho^0\rho^0$ contribution, in the following only the $\rho^0\rho^0$ content and the sum of the rest of the contributing processes, denoted as "other 4π", are considered.

To check the quality of the fit, the $\pi^+\pi^-$ mass distributions of the data are compared with those of a mixture of Monte Carlo event samples from the processes (6) and (7), in proportions determined by the fit. The data and Monte Carlo distributions are in good agreement over the entire Q^2 and $W_{\gamma\gamma}$ range. As an example $\pi^+\pi^-$ mass distributions are shown in Figure 3. The Monte Carlo production model also provides a good description of the measured angular distributions, as shown in Figure 4.

6 Results

The cross section, $\Delta\sigma_{\rm ee}$, of the process $\rm e^+e^- \to e^+e^-\rho^0\rho^0$ is measured in bins of Q^2 and $W_{\gamma\gamma}$. The results are listed in Tables 1 and 2, together with the efficiencies and the background fractions. The statistical uncertainties, listed in the Tables 1 and 2, are those of the fit. The differential cross section $d\sigma_{\rm ee}/dQ^2$, derived from $\Delta\sigma_{\rm ee}$, is listed in Table 1. When evaluating the differential cross section, a correction based on the Q^2-dependence of the $\rho^0\rho^0$ Monte Carlo sample is applied, so as to assign the cross section value to the centre of the corresponding Q^2 bin [20].

To evaluate the cross section, $\sigma_{\gamma\gamma}$, of the process $\gamma\gamma^* \to \rho^0\rho^0$, the integral of the transverse photon luminosity function, L_{TT}, is computed for each Q^2 and $W_{\gamma\gamma}$ bin using the program GALUGA [21], which performs $\mathcal{O}(\alpha^4)$ QED calculations. The cross section $\sigma_{\gamma\gamma}$ is derived from the measured cross section $\Delta\sigma_{\rm ee}$ using the relation $\Delta\sigma_{\rm ee} = L_{TT}\sigma_{\gamma\gamma}$. Thus, $\sigma_{\gamma\gamma}$ represents an effective cross section containing contributions from both transverse and longitudinal photon polarisations. The cross section of the process $\gamma\gamma^* \to \rho^0\rho^0$ is listed in Table 1 as a function of Q^2 and in Table 2 as a function of $W_{\gamma\gamma}$. The sum of the cross sections of the other contributing processes is also given in Tables 1 and 2.

Several sources of systematic uncertainty are considered. The contribution of the selection procedure, as estimated by varying the selection criteria, is in the range $4\% - 8\%$. Monte Carlo statistics give a contribution in the range $1.5\% - 2.3\%$. The variations of the acceptance observed when a ρ-pole form-factor is used instead of a GVDM form-factor for re-weighting Monte Carlo events are in the range $1\% - 3\%$ for most of the kinematic region. The uncertainties of the trigger efficiency, as determined from the data, are in the range $1.9\% - 4\%$. In order to estimate the systematic uncertainty of the fit procedure, the size and the occupancies of the boxes in the box-fit are varied, as well as the number of bins in which the data is divided for the fits. In particular, the fits in Q^2 are performed using only three bins, which results in the same integrated cross section as in the case of four Q^2 bins. A contribution of $3\% - 7\%$ is derived. Finally, an uncertainty of $2\% - 4\%$ is associated with the background determination.

All contributions are added in quadrature to obtain the systematic uncertainties quoted in Tables 1 and 2.

7 Discussion

The cross section of the process $\gamma\gamma^* \to \rho^0\rho^0$ as a function of $W_{\gamma\gamma}$ is plotted in Figure 5a, together with the sum of the cross sections of the other contributing processes. The shoulder in the latter is due to the contribution of the subprocesses involving $f_2(1270)$ production. The measured $\rho^0\rho^0$ cross section shows a broad enhancement at threshold. Figures 5b and 5c compare the measured cross sections with those measured at high Q^2 [1]. All cross sections decrease with Q^2 and the variation with Q^2 of the $\gamma\gamma^* \to \rho^0\rho^0$ cross section is more rapid for low values of $W_{\gamma\gamma}$.

The measured differential cross section $d\sigma_{\mathrm{ee}}/dQ^2$ of the reaction $\mathrm{e^+e^-} \to \mathrm{e^+e^-}\rho^0\rho^0$ is shown in Figure 6a, together with the high-Q^2 data from Reference 1. It is fitted to a form [22] expected from QCD-based calculations [23]:

$$\frac{\mathrm{d}\sigma_{\mathrm{ee}}}{\mathrm{d}Q^2} \sim \frac{1}{Q^n(Q^2 + < W_{\gamma\gamma} >^2)^2}\,, \tag{9}$$

where n is a constant and $< W_{\gamma\gamma} >$ is the average $W_{\gamma\gamma}$ value of 1.8 GeV for this measurement. Although this formula is expected to be valid only for $Q^2 \gg W_{\gamma\gamma}$, we find it provides a good parametrisation of the Q^2 evolution of all data in the interval $0.2\ \mathrm{GeV}^2 < Q^2 < 30\ \mathrm{GeV}^2$, with an exponent $n = 2.9 \pm 0.1$. In the fit, which results in $\chi^2/d.o.f. = 6.9/10$ and is shown by the line in Figure 6a, only the statistical uncertainties are considered.

The measured cross section of the process $\gamma\gamma^* \to \rho^0\rho^0$ as a function of Q^2 is shown in Figure 6b, together with the L3 data for $\rho^0\rho^0$ production at high Q^2 [1] and the PLUTO measurement for $1\ \mathrm{GeV} < W_{\gamma\gamma} < 3.2\ \mathrm{GeV}$ [5]. The two data sets agree for $Q^2 > 0.3\ \mathrm{GeV}^2$ while for low Q^2 values the L3 data lie below the PLUTO measurement. The L3 data is fitted with a form-factor parametrisation based on the GVDM model [12], which is found to reproduce well the Q^2 dependence of our measurements. Only the statistical uncertainties are considered in the fit, which results in $\chi^2/d.o.f. = 7.5/11$. Figure 6b also shows the result of a ρ-pole form-factor fit to the PLUTO data, as in reference 5. The L3 data cannot be described by the steeper fall of the ρ-pole parametrisation.

References

[1] L3 Coll., P. Achard *et al.*, Phys. Lett. B **568** (2003) 11.

[2] L3 Coll., P. Achard *et al.*, Phys. Lett. B **597** (2004) 26.

[3] ARGUS Coll., H. Albrecht *et al.*, Phys. Lett. B **217** (1989) 205; Phys. Lett. B **267** (1991) 535; CELLO Coll., H.-J. Behrend *et al.*, Phys. Lett. B **218** (1989) 493.

[4] TASSO Coll., R. Brandelik *et al.*, Phys. Lett. B **97** (1980) 448; M. Althoff *et al.*, Z. Phys. C **16** (1982) 13; MARK II Coll., D.L. Burke *et al.*, Phys. Lett. B **103** (1981) 153; CELLO Coll., H.-J. Behrend *et al.*, Z. Phys. C **21** (1984) 205; TPC/Two-Gamma Coll., H. Aihara *et al.*, Phys. Rev. D **37** (1988) 28; ARGUS Coll., H. Albrecht *et al.*, Z. Phys. C **50** (1991) 1.

[5] PLUTO Coll., Ch. Berger *et al.*, Z. Phys. C **38** (1988) 521.

[6] M. Diehl *et al.*, Phys. Rev. Lett. **81** (1998) 1782; N. Kivel, L. Mankiewicz and M.V. Polyakov, Phys. Lett. B **467** (1999) 263; A. Freund, Phys. Rev. D **61** (2000) 074010.

[7] I.V. Anikin, B. Pire and O.V. Teryaev, Phys. Rev. D **69** (2004) 014018.

[8] N.N. Achasov *et al.*, Phys. Lett. B **108** (1982) 134; Z. Phys. C **16** (1982) 55; Phys. Lett. B **203** (1988) 309; G. Alexander *et al.*, Phys. Rev. D **26** (1982) 1198; Z. Phys. C **30** (1986) 65; B.A. Li and K.F. Liu, Phys. Lett. B **118** (1982) 435; Phys. Lett. B **124** (1983) 550; Phys. Rev. D **30** (1984) 613; Phys. Rev. Lett. **58** (1987) 2288; S.J. Brodsky, G. Köpp and P.M. Zerwas, Phys. Rev. Lett. **58** (1987) 443.

[9] J.L. Rosner Phys. Rev. **D 70** (2004) 034028.

[10] L3 Coll., B. Adeva *et al.*, Nucl. Instr. Meth. A **289** (1990) 35; M. Chemarin *et al.*, Nucl. Instr. Meth. A **349** (1994) 345; M. Acciarri *et al.*, Nucl. Instr. Meth. A **351** (1994) 300; I.C. Brock *et al.*, Nucl. Instr. Meth. A **381** (1996) 236; A. Adam *et al.*, Nucl. Instr. Meth. A **383** (1996) 342.

[11] T. van Rhee, Ph.D. thesis, University of Ultrecht (1999).

[12] J.J. Sakurai and D. Schildknecht, Phys. Lett. B **40** (1972) 121; I.F. Ginzburg and V.G. Serbo, Phys. Lett. B **109** (1982) 231.

[13] P. Béné *et al.*, Nucl. Instr. Meth. A **306** (1991) 150; D. Haas *et al.*, Nucl. Instr. Meth. A **420** (1999) 101.

[14] F.L. Linde, Ph.D. thesis, Rijksuniversiteit Leiden (1988).

[15] V.M. Budnev *et al.*, Phys. Rep. C **15** (1975) 181.

[16] GEANT version 3.21 is used; R. Brun *et al.*, CERN report CERN DD/EE/84-1 (1984), revised 1987.

[17] GEISHA, H. Fesefeldt, RWTH Aachen report PITHA 85/2 (1985).

[18] LEP4F version 2.0 is used; J.A.M. Vermaseren *et al.*, Phys. Rev. D **19** (1979) 137; J.A.M. Vermaseren, Nucl. Phys. B **229** (1983) 347.

[19] D.M. Schmidt, R.J. Morrison and M.S. Witherell, Nucl. Instr. Meth. A **328** (1993) 547.

[20] G.D. Lafferty and T.R. Wyatt, Nucl. Instr. Meth. A **355** (1995) 541.

[21] G.A. Schuler, Comput. Phys. Commun. **108** (1998) 279.

[22] M. Diehl, private communication.

[23] M. Diehl, T. Gousset and B. Pire, Phys. Rev. D **62** (2000) 073014.

The L3 Collaboration:

P.Achard,[20] O.Adriani,[17] M.Aguilar-Benitez,[25] J.Alcaraz,[25] G.Alemanni,[23] J.Allaby,[18] A.Aloisio,[29] M.G.Alviggi,[29] H.Anderhub,[49] V.P.Andreev,[6,34] F.Anselmo,[8] A.Arefiev,[28] T.Azemoon,[3] T.Aziz,[9] P.Bagnaia,[39] A.Bajo,[25] G.Baksay,[26] L.Baksay,[26] S.V.Baldew,[2] S.Banerjee,[9] Sw.Banerjee,[4] A.Barczyk,[49,47] R.Barillère,[18] P.Bartalini,[23] M.Basile,[8] N.Batalova,[46] R.Battiston,[33] A.Bay,[23] F.Becattini,[17] U.Becker,[13] F.Behner,[49] L.Bellucci,[17] R.Berbeco,[3] J.Berdugo,[25] P.Berges,[13] B.Bertucci,[33] B.L.Betev,[49] M.Biasini,[33] M.Biglietti,[29] A.Biland,[49] J.J.Blaising,[4] S.C.Blyth,[35] G.J.Bobbink,[2] A.Böhm,[1] L.Boldizsar,[12] B.Borgia,[39] S.Bottai,[17] D.Bourilkov,[49] M.Bourquin,[20] S.Braccini,[20] J.G.Branson,[41] F.Brochu,[4] J.D.Burger,[13] W.J.Burger,[33] X.D.Cai,[13] M.Capell,[13] G.Cara Romeo,[8] G.Carlino,[29] A.Cartacci,[17] J.Casaus,[25] F.Cavallari,[39] N.Cavallo,[36] C.Cecchi,[33] M.Cerrada,[25] M.Chamizo,[20] Y.H.Chang,[44] M.Chemarin,[24] A.Chen,[44] G.Chen,[7] G.M.Chen,[7] H.F.Chen,[22] H.S.Chen,[7] G.Chiefari,[29] L.Cifarelli,[40] F.Cindolo,[8] I.Clare,[13] R.Clare,[38] G.Coignet,[4] N.Colino,[25] S.Costantini,[39] B.de la Cruz,[25] S.Cucciarelli,[33] R.de Asmundis,[29] P.Déglon,[20] J.Debreczeni,[12] A.Degré,[4] K.Dehmelt,[26] K.Deiters,[47] D.della Volpe,[29] E.Delmeire,[20] P.Denes,[37] F.DeNotaristefani,[39] A.De Salvo,[49] M.Diemoz,[39] M.Dierckxsens,[2] C.Dionisi,[39] M.Dittmar,[49] A.Doria,[29] M.T.Dova,[10,♯] D.Duchesneau,[4] M.Duda,[1] B.Echenard,[20] A.Eline,[18] A.El Hage,[1] H.El Mamouni,[24] A.Engler,[35] F.J.Eppling,[13] P.Extermann,[20] M.A.Falagan,[25] S.Falciano,[39] A.Favara,[32] J.Fay,[24] O.Fedin,[34] M.Felcini,[49] T.Ferguson,[35] H.Fesefeldt,[1] E.Fiandrini,[33] J.H.Field,[20] F.Filthaut,[31] P.H.Fisher,[13] W.Fisher,[37] I.Fisk,[41] G.Forconi,[13] K.Freudenreich,[49] C.Furetta,[27] Yu.Galaktionov,[28,13] S.N.Ganguli,[9] P.Garcia-Abia,[25] M.Gataullin,[32] S.Gentile,[39] S.Giagu,[39] Z.F.Gong,[22] G.Grenier,[24] O.Grimm,[49] M.W.Gruenewald,[16] M.Guida,[40] V.K.Gupta,[37] A.Gurtu,[9] L.J.Gutay,[46] D.Haas,[5] D.Hatzifotiadou,[8] T.Hebbeker,[1] A.Hervé,[18] J.Hirschfelder,[35] H.Hofer,[49] M.Hohlmann,[26] G.Holzner,[49] S.R.Hou,[44] B.N.Jin,[7] P.Jindal,[14] L.W.Jones,[3] P.de Jong,[2] I.Josa-Mutuberría,[25] M.Kaur,[14] M.N.Kienzle-Focacci,[20] J.K.Kim,[43] J.Kirkby,[18] W.Kittel,[31] A.Klimentov,[13,28] A.C.König,[31] M.Kopal,[46] V.Koutsenko,[13,28] M.Kräber,[49] R.W.Kraemer,[35] A.Krüger,[48] A.Kunin,[13] P.Ladron de Guevara,[25] I.Laktineh,[24] G.Landi,[17] M.Lebeau,[18] A.Lebedev,[13] P.Lebrun,[24] P.Lecomte,[49] P.Lecoq,[18] P.Le Coultre,[49] J.M.Le Goff,[18] R.Leiste,[48] M.Levtchenko,[27] P.Levtchenko,[34] C.Li,[22] S.Likhoded,[48] C.H.Lin,[44] W.T.Lin,[44] F.L.Linde,[2] L.Lista,[29] Z.A.Liu,[7] W.Lohmann,[48] E.Longo,[39] Y.S.Lu,[7] C.Luci,[39] L.Luminari,[39] W.Lustermann,[49] W.G.Ma,[22] L.Malgeri,[18] A.Malinin,[28] C.Maña,[25] J.Mans,[37] J.P.Martin,[24] F.Marzano,[39] K.Mazumdar,[9] R.R.McNeil,[6] S.Mele,[18,29] L.Merola,[29] M.Meschini,[17] W.J.Metzger,[31] A.Mihul,[11] H.Milcent,[18] G.Mirabelli,[39] J.Mnich,[1] G.B.Mohanty,[9] G.S.Muanza,[24] A.J.M.Muijs,[2] B.Musicar,[41] M.Musy,[39] S.Nagy,[15] S.Natale,[20] M.Napolitano,[29] F.Nessi-Tedaldi,[49] H.Newman,[32] A.Nisati,[39] T.Novak,[31] H.Nowak,[48] R.Ofierzynski,[49] G.Organtini,[39] I.Pal,[46] C.Palomares,[25] P.Paolucci,[29] R.Paramatti,[39] G.Passaleva,[17] S.Patricelli,[29] T.Paul,[10] M.Pauluzzi,[33] C.Paus,[13] F.Pauss,[49] M.Pedace,[39] S.Pensotti,[27] D.Perret-Gallix,[4] D.Piccolo,[29] F.Pierella,[8] M.Pioppi,[33] P.A.Piroué,[37] E.Pistolesi,[27] V.Plyaskin,[28] M.Pohl,[20] V.Pojidaev,[17] J.Pothier,[18] D.Prokofiev,[34] J.Quartieri,[40] G.Rahal-Callot,[49] M.A.Rahaman,[9] P.Raics,[15] N.Raja,[9] R.Ramelli,[49] P.G.Rancoita,[27] R.Ranieri,[17] A.Raspereza,[48] P.Razis,[30] D.Ren,[49] M.Rescigno,[39] S.Reucroft,[10] S.Riemann,[48] K.Riles,[3] B.P.Roe,[3] L.Romero,[25] A.Rosca,[48] C.Rosemann,[1] C.Rosenbleck,[1] S.Rosier-Lees,[4] S.Roth,[1] J.A.Rubio,[18] G.Ruggiero,[17] H.Rykaczewski,[49] A.Sakharov,[49] S.Saremi,[6] S.Sarkar,[39] J.Salicio,[18] E.Sanchez,[25] C.Schäfer,[18] V.Schegelsky,[34] H.Schopper,[21] D.J.Schotanus,[31] C.Sciacca,[29] L.Servoli,[33] S.Shevchenko,[32] N.Shivarov,[42] V.Shoutko,[13] E.Shumilov,[28] A.Shvorob,[32] D.Son,[43] C.Souga,[24] P.Spillantini,[17] M.Steuer,[13] D.P.Stickland,[37] B.Stoyanov,[42] A.Straessner,[20] K.Sudhakar,[9] G.Sultanov,[42] L.Z.Sun,[22] S.Sushkov,[1] H.Suter,[49] J.D.Swain,[10] Z.Szillasi,[26,¶] X.W.Tang,[7] P.Tarjan,[15] L.Tauscher,[5] L.Taylor,[10] B.Tellili,[24] D.Teyssier,[24] C.Timmermans,[31] Samuel C.C.Ting,[13] S.M.Ting,[13] S.C.Tonwar,[9] J.Tóth,[12] C.Tully,[37] K.L.Tung,[7] J.Ulbricht,[49] E.Valente,[39] R.T.Van de Walle,[31] R.Vasquez,[46] V.Veszpremi,[26] G.Vesztergombi,[12] I.Vetlitsky,[28] D.Vicinanza,[40] G.Viertel,[49] S.Villa,[38] M.Vivargent,[4] S.Vlachos,[5] I.Vodopianov,[26] H.Vogel,[35] H.Vogt,[48] I.Vorobiev,[35,28] A.A.Vorobyov,[34] M.Wadhwa,[5] Q.Wang,[31] X.L.Wang,[22] Z.M.Wang,[22] M.Weber,[18] S.Wynhoff,[37] L.Xia,[32] Z.Z.Xu,[22] J.Yamamoto,[3] B.Z.Yang,[22] C.G.Yang,[7] H.J.Yang,[3] M.Yang,[7] S.C.Yeh,[45] An.Zalite,[34] Yu.Zalite,[34] Z.P.Zhang,[22] J.Zhao,[22] G.Y.Zhu,[7] R.Y.Zhu,[32] H.L.Zhuang,[7] A.Zichichi,[8,18,19] B.Zimmermann,[49] M.Zöller.[1]

1 III. Physikalisches Institut, RWTH, D-52056 Aachen, Germany[§]
2 National Institute for High Energy Physics, NIKHEF, and University of Amsterdam, NL-1009 DB Amsterdam, The Netherlands
3 University of Michigan, Ann Arbor, MI 48109, USA
4 Laboratoire d'Annecy-le-Vieux de Physique des Particules, LAPP,IN2P3-CNRS, BP 110, F-74941 Annecy-le-Vieux CEDEX, France
5 Institute of Physics, University of Basel, CH-4056 Basel, Switzerland
6 Louisiana State University, Baton Rouge, LA 70803, USA
7 Institute of High Energy Physics, IHEP, 100039 Beijing, China[△]
8 University of Bologna and INFN-Sezione di Bologna, I-40126 Bologna, Italy
9 Tata Institute of Fundamental Research, Mumbai (Bombay) 400 005, India
10 Northeastern University, Boston, MA 02115, USA
11 Institute of Atomic Physics and University of Bucharest, R-76900 Bucharest, Romania
12 Central Research Institute for Physics of the Hungarian Academy of Sciences, H-1525 Budapest 114, Hungary[‡]
13 Massachusetts Institute of Technology, Cambridge, MA 02139, USA
14 Panjab University, Chandigarh 160 014, India
15 KLTE-ATOMKI, H-4010 Debrecen, Hungary[¶]
16 Department of Experimental Physics, University College Dublin, Belfield, Dublin 4, Ireland
17 INFN Sezione di Firenze and University of Florence, I-50125 Florence, Italy
18 European Laboratory for Particle Physics, CERN, CH-1211 Geneva 23, Switzerland
19 World Laboratory, FBLJA Project, CH-1211 Geneva 23, Switzerland
20 University of Geneva, CH-1211 Geneva 4, Switzerland
21 University of Hamburg, D-22761 Hamburg, Germany
22 Chinese University of Science and Technology, USTC, Hefei, Anhui 230 029, China[△]
23 University of Lausanne, CH-1015 Lausanne, Switzerland
24 Institut de Physique Nucléaire de Lyon, IN2P3-CNRS,Université Claude Bernard, F-69622 Villeurbanne, France
25 Centro de Investigaciones Energéticas, Medioambientales y Tecnológicas, CIEMAT, E-28040 Madrid, Spain[♭]
26 Florida Institute of Technology, Melbourne, FL 32901, USA
27 INFN-Sezione di Milano, I-20133 Milan, Italy
28 Institute of Theoretical and Experimental Physics, ITEP, Moscow, Russia
29 INFN-Sezione di Napoli and University of Naples, I-80125 Naples, Italy
30 Department of Physics, University of Cyprus, Nicosia, Cyprus
31 Radboud University and NIKHEF, NL-6525 ED Nijmegen, The Netherlands
32 California Institute of Technology, Pasadena, CA 91125, USA
33 INFN-Sezione di Perugia and Università Degli Studi di Perugia, I-06100 Perugia, Italy
34 Nuclear Physics Institute, St. Petersburg, Russia
35 Carnegie Mellon University, Pittsburgh, PA 15213, USA
36 INFN-Sezione di Napoli and University of Potenza, I-85100 Potenza, Italy
37 Princeton University, Princeton, NJ 08544, USA
38 University of Californa, Riverside, CA 92521, USA
39 INFN-Sezione di Roma and University of Rome, "La Sapienza", I-00185 Rome, Italy
40 University and INFN, Salerno, I-84100 Salerno, Italy
41 University of California, San Diego, CA 92093, USA
42 Bulgarian Academy of Sciences, Central Lab. of Mechatronics and Instrumentation, BU-1113 Sofia, Bulgaria
43 The Center for High Energy Physics, Kyungpook National University, 702-701 Taegu, Republic of Korea
44 National Central University, Chung-Li, Taiwan, China
45 Department of Physics, National Tsing Hua University, Taiwan, China
46 Purdue University, West Lafayette, IN 47907, USA
47 Paul Scherrer Institut, PSI, CH-5232 Villigen, Switzerland
48 DESY, D-15738 Zeuthen, Germany
49 Eidgenössische Technische Hochschule, ETH Zürich, CH-8093 Zürich, Switzerland
§ Supported by the German Bundesministerium für Bildung, Wissenschaft, Forschung und Technologie.
‡ Supported by the Hungarian OTKA fund under contract numbers T019181, F023259 and T037350.
¶ Also supported by the Hungarian OTKA fund under contract number T026178.
♭ Supported also by the Comisión Interministerial de Ciencia y Tecnología.
♯ Also supported by CONICET and Universidad Nacional de La Plata, CC 67, 1900 La Plata, Argentina.
△ Supported by the National Natural Science Foundation of China.

Q^2 range [GeV^2]	ε [%]	Bg [%]	$\Delta\sigma_{ee}$ [pb] $\rho^0\rho^0$	$d\,\sigma_{ee}/d\,Q^2$ [pb / GeV^2] $\rho^0\rho^0$	$\sigma_{\gamma\gamma}$ [nb] $\rho^0\rho^0$	$\sigma_{\gamma\gamma}$ [nb] other 4π
0.20 – 0.28	2.4	8	$12.5 \pm 1.18 \pm 0.79$	$155 \pm 15 \pm 10$	$9.65 \pm 0.92 \pm 0.62$	$15.6 \pm 1.19 \pm 0.90$
0.28 – 0.40	3.7	9	$10.9 \pm 0.90 \pm 0.72$	$89.5 \pm 7.4 \pm 5.9$	$8.18 \pm 0.68 \pm 0.54$	$13.0 \pm 0.89 \pm 0.86$
0.40 – 0.55	3.0	12	$6.37 \pm 0.78 \pm 0.54$	$42.1 \pm 5.1 \pm 3.6$	$5.59 \pm 0.68 \pm 0.47$	$12.7 \pm 0.94 \pm 0.90$
0.55 – 0.85	2.0	20	$6.80 \pm 0.95 \pm 0.83$	$22.1 \pm 3.1 \pm 2.7$	$4.63 \pm 0.65 \pm 0.57$	$7.86 \pm 0.81 \pm 0.79$

Table 1: Detection efficiencies, ε, background fractions, Bg, and measured production cross sections of the reactions $e^+e^- \to e^+e^-\rho^0\rho^0$, $\gamma\gamma^* \to \rho^0\rho^0$ and of the sum of the rest of the contributing processes, other 4π, as a function of Q^2 for 1.1 GeV $< W_{\gamma\gamma} <$ 3 GeV. The values of the differential cross sections are corrected to the centre of each bin. The first uncertainties are statistical, the second systematic.

$W_{\gamma\gamma}$-range [GeV]	ε [%]	Bg [%]	$\Delta\sigma_{ee}$ [pb] $\rho^0\rho^0$	$\sigma_{\gamma\gamma}$ [nb] $\rho^0\rho^0$	$\sigma_{\gamma\gamma}$ [nb] other 4π
1.10 – 1.30	1.8	15	$6.94 \pm 1.08 \pm 0.77$	$8.05 \pm 1.25 \pm 0.89$	$7.94 \pm 1.43 \pm 0.86$
1.30 – 1.45	2.6	12	$6.81 \pm 0.85 \pm 0.58$	$11.8 \pm 1.48 \pm 1.01$	$14.3 \pm 1.83 \pm 1.28$
1.45 – 1.60	2.8	9	$7.07 \pm 0.81 \pm 0.62$	$13.5 \pm 1.55 \pm 1.19$	$15.9 \pm 1.83 \pm 1.30$
1.60 – 1.75	3.1	10	$5.61 \pm 0.70 \pm 0.47$	$11.8 \pm 1.46 \pm 0.99$	$16.4 \pm 1.77 \pm 1.24$
1.75 – 1.90	3.1	10	$3.56 \pm 0.57 \pm 0.36$	$8.17 \pm 1.32 \pm 0.83$	$18.1 \pm 1.86 \pm 1.58$
1.90 – 2.10	3.1	11	$3.37 \pm 0.56 \pm 0.38$	$6.38 \pm 1.07 \pm 0.71$	$14.0 \pm 1.40 \pm 1.13$
2.10 – 2.50	3.2	11	$2.25 \pm 0.44 \pm 0.27$	$2.48 \pm 0.49 \pm 0.30$	$14.1 \pm 1.07 \pm 0.96$
2.50 – 3.00	3.1	11	$0.93 \pm 0.28 \pm 0.12$	$1.01 \pm 0.31 \pm 0.13$	$6.85 \pm 0.70 \pm 0.61$

Table 2: Detection efficiencies, ε, background fractions, Bg, and measured production cross sections of the reactions $e^+e^- \to e^+e^-\rho^0\rho^0$, $\gamma\gamma^* \to \rho^0\rho^0$ and of the sum of the rest of the contributing processes, other 4π, as a function of $W_{\gamma\gamma}$ for $0.2\ \mathrm{GeV}^2 < Q^2 < 0.85\ \mathrm{GeV}^2$. The first uncertainties are statistical, the second systematic.

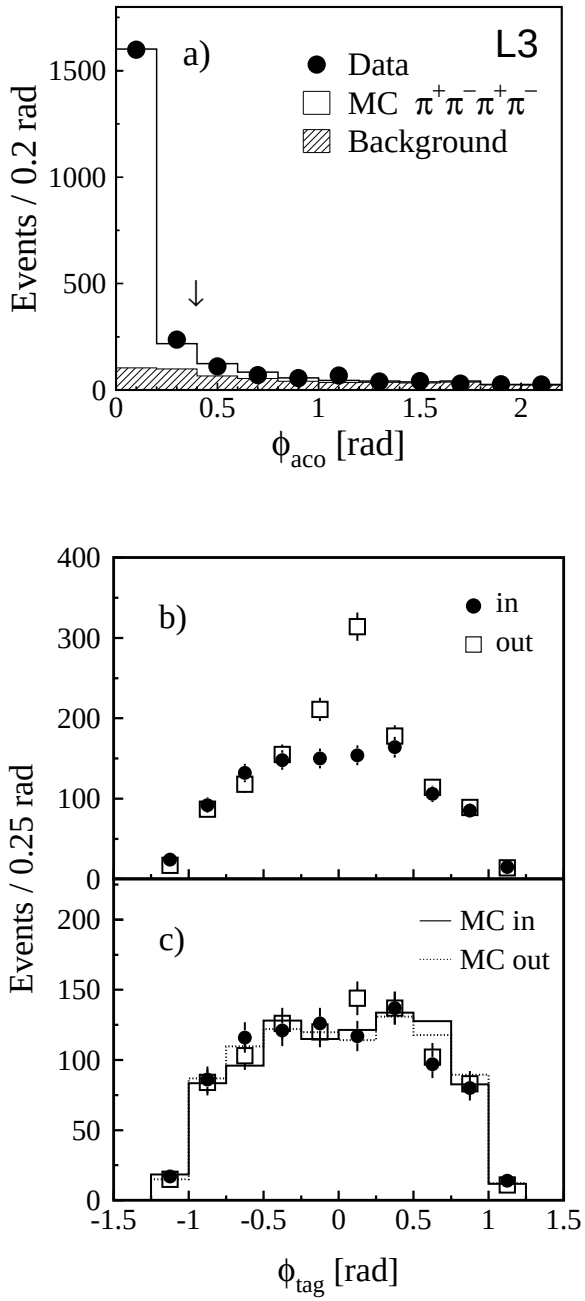

Figure 1: (a) Distribution of the acoplanarity angle, ϕ_{aco}, between the electron and the $\pi^+\pi^-\pi^+\pi^-$ system for data (points) compared to the four-pion Monte Carlo (open histogram) and the background estimated from the data (hatched histogram). The arrow indicates the selection cut. The shapes of the Monte Carlo and the background are fixed, and their sum is normalised to the total number of events. (b) and (c) Distributions of the azimuthal angle of the tagged electron in the selected events, ϕ_{tag}, for electrons in the inner side of the LEP ring (in) and, folded over it, distributions for electrons in the outer side of the LEP ring (out). In (b) all cuts but the acoplanarity cut are applied and in (c) all cuts are applied and the corresponding four-pion Monte Carlo distributions are also shown.

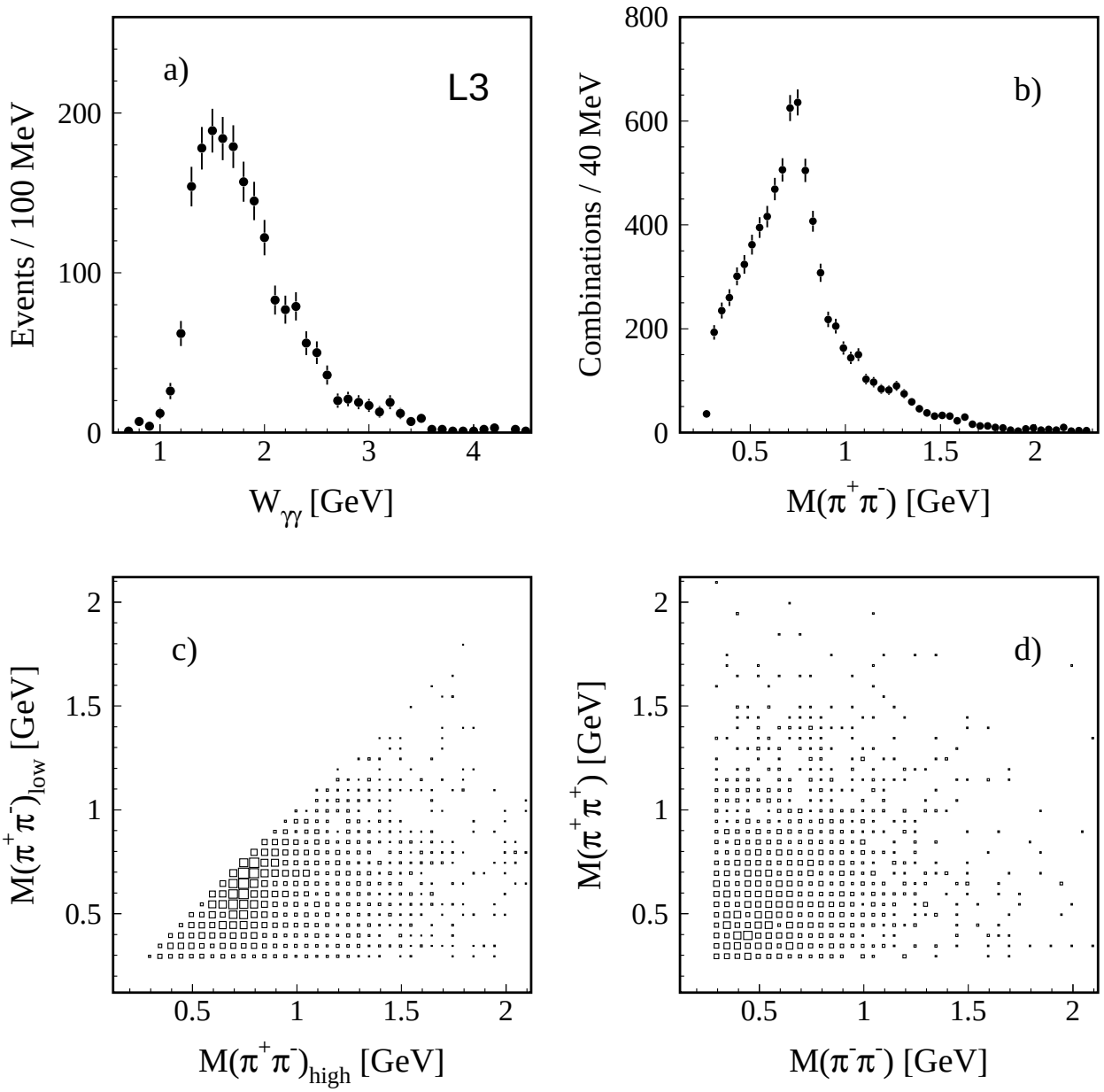

Figure 2: Mass distributions for the selected events. (a) Mass of the four-pion system, $W_{\gamma\gamma}$. (b) Mass of $\pi^+\pi^-$ combinations (four entries per event). (c) Correlation between the lower versus higher mass combinations of the $\pi^+\pi^-$ pairs (two entries per event). (d) Correlation between the masses of the $\pi^+\pi^+$ and $\pi^-\pi^-$ pairs. The two-dimensional plots in (c) and (d) have a bin width of 50×50 MeV^2 and the size of the squares is proportional to the number of entries.

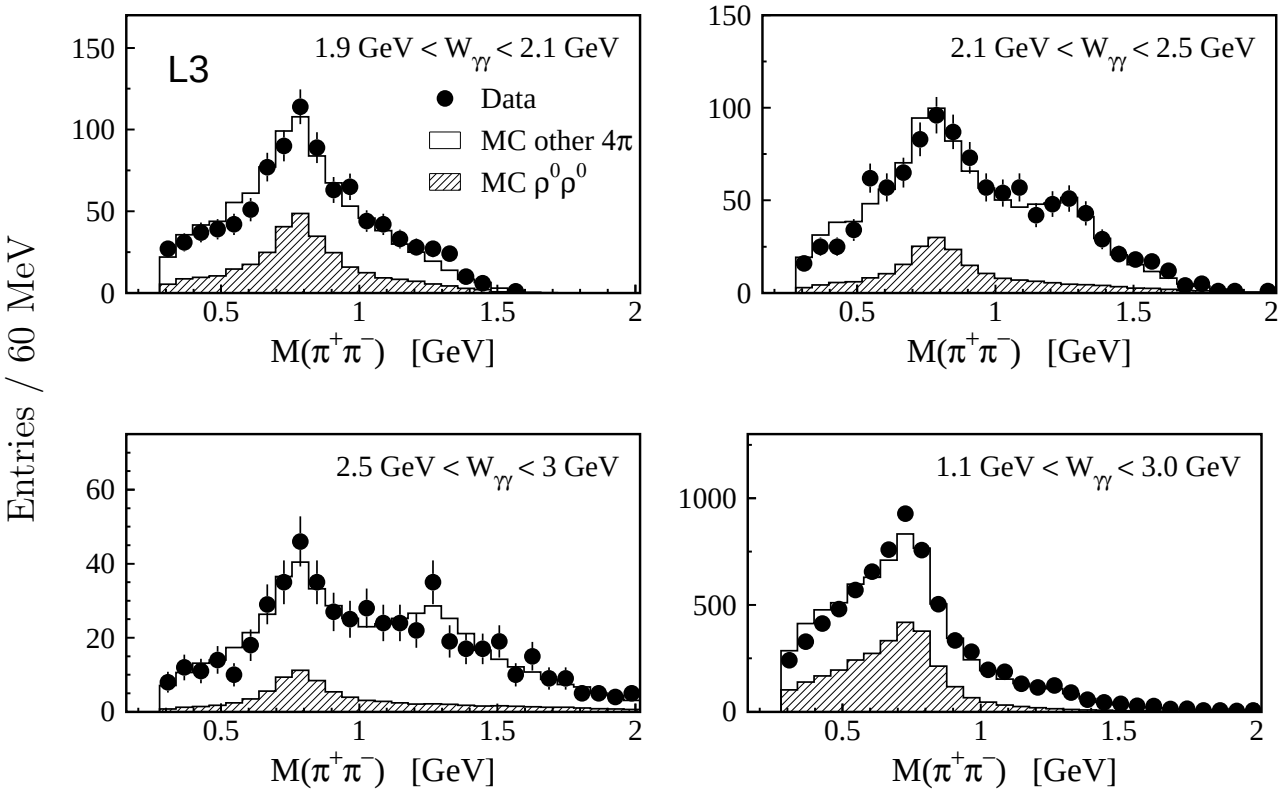

Figure 3: Mass distributions of $\pi^+\pi^-$ combinations (four entries per event) for the three higher $W_{\gamma\gamma}$ intervals and for the total sample for 0.2 GeV^2 $< Q^2 <$ 0.85 GeV^2. The points represent the data, the hatched area shows the $\rho^0\rho^0$ component and the open area shows the sum of the rest of the contributing processes. The fraction of the different components are determined by the fit and the normalisation is to the total number of events. The plot for the entire $W_{\gamma\gamma}$ range, 1.1 GeV $< W_{\gamma\gamma} <$ 3 GeV, is a sum of the distributions of all fitted $W_{\gamma\gamma}$ intervals.

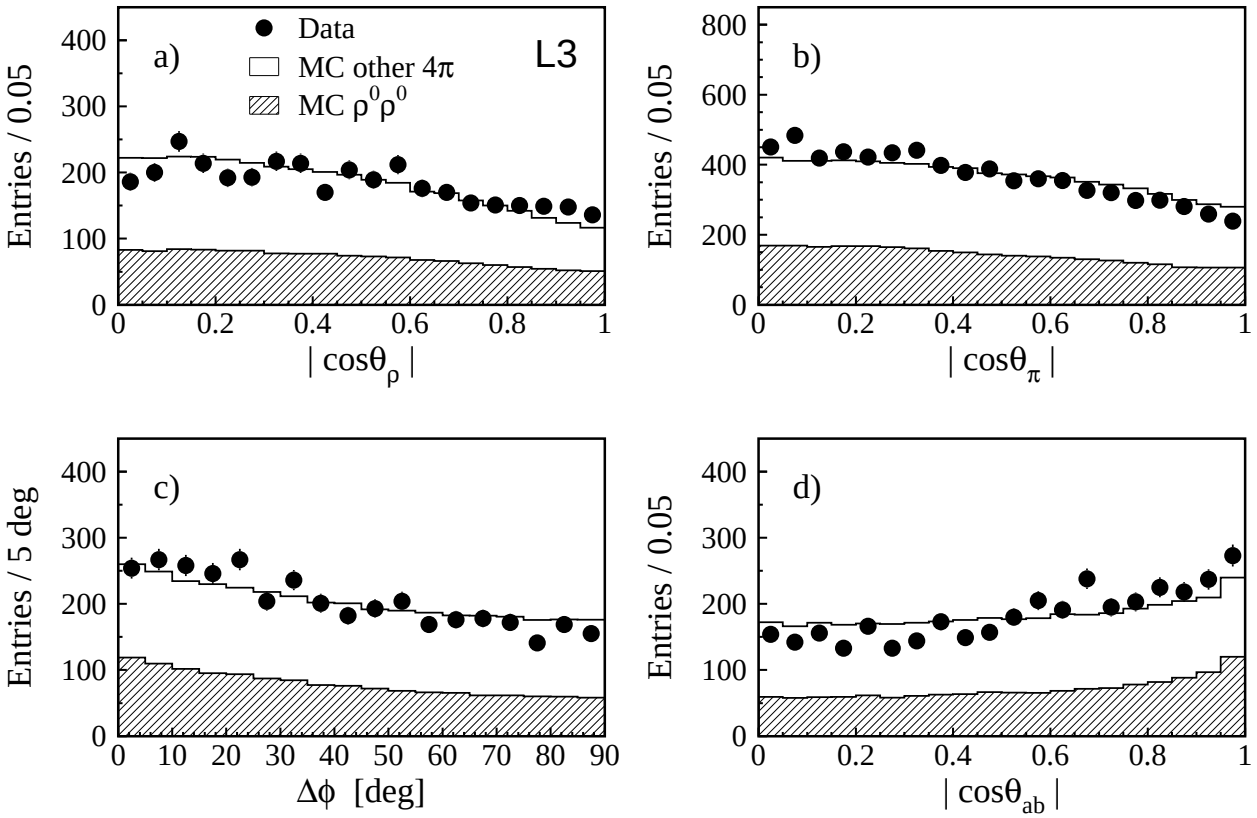

Figure 4: Comparison of the data and Monte Carlo angular distributions for the kinematic regions (1) and (2): (a) $|\cos\theta_\rho|$, the cosine of the polar angle of the ρ^0 with respect to the $\gamma\gamma^*$ axis in the $\gamma\gamma^*$ centre-of-mass system; (b) $|\cos\theta_\pi|$, the cosine of the polar angle of the pion in its parent ρ^0 helicity-system; (c) $\Delta\phi$, the angle between the decay planes of the two ρ^0 mesons in the $\gamma\gamma^*$ centre-of-mass system; (d) $|\cos\theta_{\rm ab}|$, the cosine of the opening angle between the two π^+ directions of flight, each one defined in its parent ρ^0 helicity-system. There are two entries per event in (a), (c) and (d) and four entries per event in (b). The points represent data, the hatched area shows the $\rho^0\rho^0$ component and the open area shows the sum of the rest of the contributing processes. The fraction of the different components are determined by the fit and the normalisation is to the total number of events.

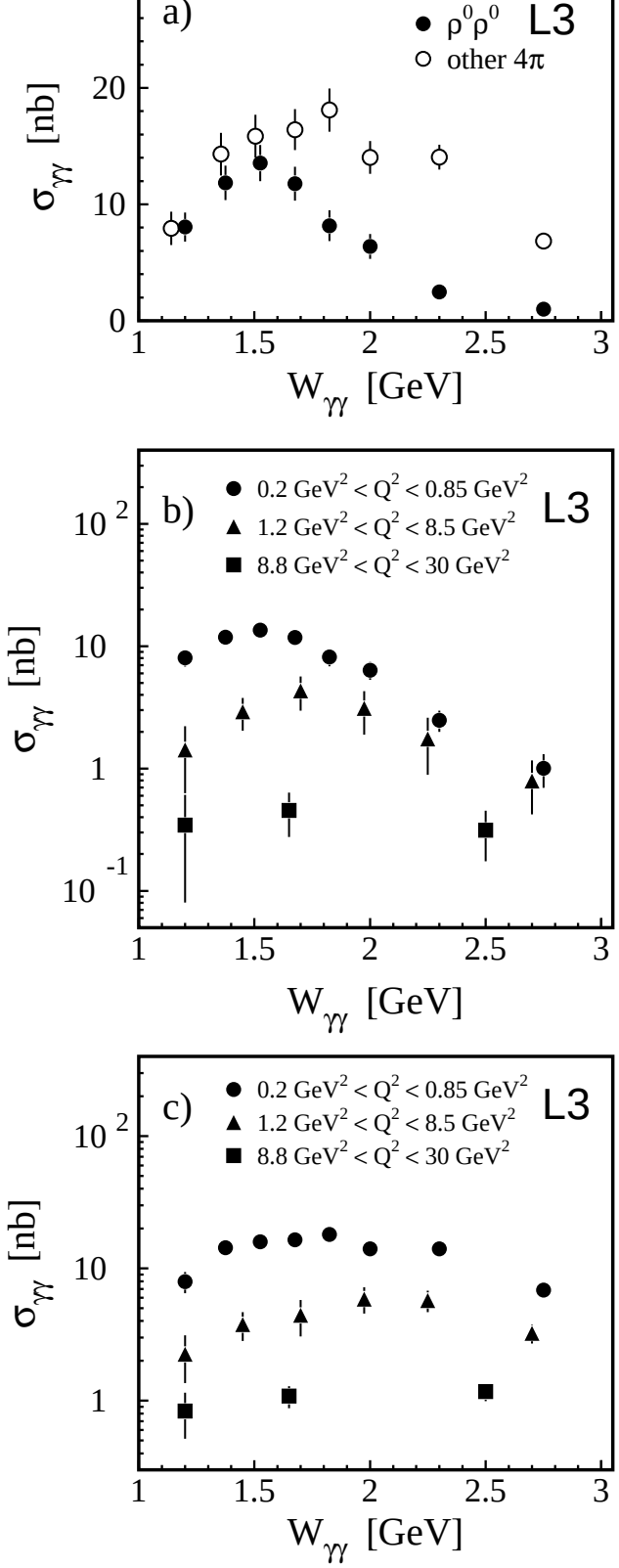

Figure 5: (a) Cross section of the process $\gamma\gamma^* \to \rho^0\rho^0$ (full points) and the sum of the rest of the contributing processes (open points), as a function of $W_{\gamma\gamma}$ for 0.2 GeV^2 < Q^2 < 0.85 GeV^2. The bars show the statistical uncertainties. The two sets of points have the same binning and some points are horizontally displaced for better legibility. Comparison of the results of this measurement and that at high Q^2 [1] for (b) the $\gamma\gamma^* \to \rho^0\rho^0$ process and (c) the sum of the rest of the contributing processes.

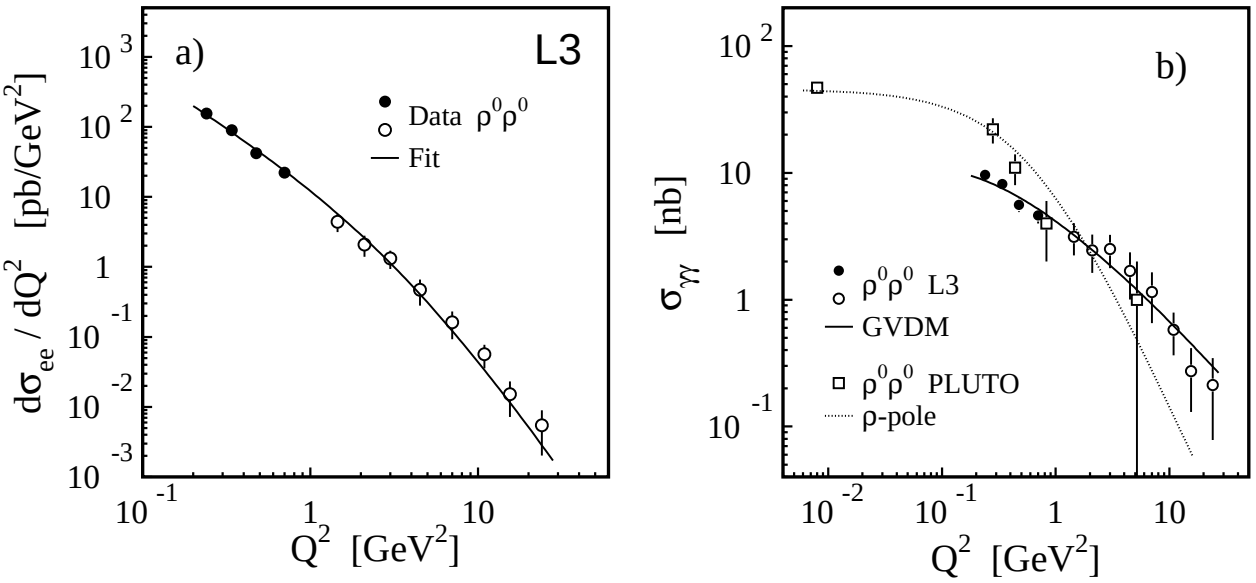

Figure 6: The $\rho^0\rho^0$ production cross section as a function of Q^2: (a) differential cross section of the process $e^+e^- \to e^+e^-\rho^0\rho^0$ and (b) cross section of the process $\gamma\gamma^* \to \rho^0\rho^0$. The full points show the results from this measurement, the open points show the results from the L3 measurement of $\rho^0\rho^0$ production at high Q^2 [1] and the squares in (b) show the results from the PLUTO measurement [5]. The bars show the statistical uncertainties. The L3 measurements are for the interval 1.1 GeV $< W_{\gamma\gamma} <$ 3 GeV and the PLUTO measurements for 1 GeV $< W_{\gamma\gamma} <$ 3.2 GeV. The line in (a) represents the result of a fit using the QCD-inspired form of equation (9). The solid line in (b) represents the result of a fit to the L3 data based on the GVDM model [12] and the dotted line indicates the result of a fit to the PLUTO data using a ρ-pole form-factor.